Yousefi et al., *BioImpacts.* 2025;15:30247
doi: 10.34172/bi.30247
https://bi.tbzmed.ac.ir/

Critical-size bone defect repair with three types of nano-hydroxyapatite scaffolds: An *in vivo* study

Mohammad Yousefi[1,2,3], Nicola Maffulli[4,5,6], Marjan Bahraminasab[7,8*], Samaneh Arab[8], Akram Alizadeh[7,8], Ali Ghanbari[9], Athar Talebi[8], Muhammad Mehdi Jafari Sorkhdehi[1,10]

[1]Student Research Committee, Semnan University of Medical Sciences, Semnan, Iran
[2]Department of Medicine, School of Medicine, Semnan University of Medical Sciences, Semnan, Iran
[3]Skull Base Research Center, The Five Senses Health Institute, School of Medicine, Iran University of Medical Sciences, Tehran, Iran
[4]Department of Medicine, Surgery and Dentistry, University of Salerno, Baronissi, SA, Italy
[5]Barts and the London School of Medicine and Dentistry, Centre for Sports and Exercise Medicine, Queen Mary University of London, London, UK
[6]School of Pharmacy and Bioengineering, Keele University Faculty of Medicine, Stoke on Trent, UK
[7]Nervous System Stem Cells Research Center, Semnan University of Medical Sciences, Semnan, Iran
[8]Department of Tissue Engineering and Applied Cell Sciences, School of Medicine, Semnan University of Medical Sciences, Semnan, Iran
[9]Research Center of Physiology, Semnan University of Medical Sciences, Semnan, Iran
[10]Department of Medicine, School of Medicine, Semnan University of Medical Sciences, Semnan, Iran

Article Info

Article Type:
Original Article

Article History:
Received: 30 Dec. 2023
Revised: 2 Aug. 2024
Accepted: 8 Jan. 2025
ePublished: 1 Mar. 2025

Keywords:
Nano hydroxyapatite
Carp
Biocompatibility
Rat skull
Bone defect
In vivo

Abstract

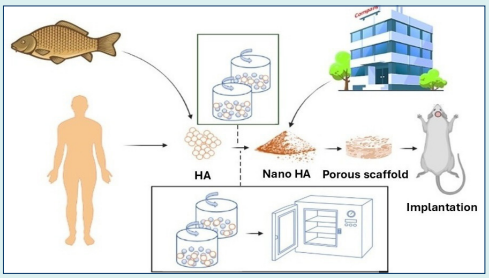

Introduction: Hydroxyapatite (HA), the main mineral component of bone, can be synthesized and utilized in the bone lesion treatments because of its high bioactivity and osteoconductive property. HA extraction from fish bones has received special attention given its low cost and easier extraction protocol compared to other sources. The present study compared the biocompatibility and bone repair of commercial nano hydroxyapatite (nHA) powder with that extracted from carp and human bones *in vitro* and *in vivo*.

Methods: First, nHA powders were prepared, and their physical and structural properties were studied using XRD, FTIR, FE-SEM and EDS analyses. Next, the powders were used to make porous scaffolds for which the physicochemical, structural, mechanical and biological properties were evaluated. The *in vitro* biocompatibility and osteogenic differentiation were tested on MC3T3-E1 cells, respectively, by MTT assay in three time periods and Alizarin red staining. Furthermore, the scaffolds were implanted after creation of critical-size lesions in the skulls of female rats, and the histological investigation was conducted by H&E staining at two time points.

Results: The morphological and phase analyses showed the successful fabrication of porous nHA scaffolds with 60.68%, 61.38, and 63.27% for carp, human and commercial nHA scaffolds, respectively. The scaffolds showed different biodegradability behavior where the human nHA scaffolds degrade more rapidly. The results of mechanical tests indicated that the scaffolds made up of human extracted nHA powder had the lowest strength and stiffness (3.13 and 37.37 KPa, respectively). The strength and stiffness of the scaffolds fabricated by carp extracted and commercial nHA were 17.14 and 19.01 Kpa, and 251.79 and 140.49 Kpa, respectively. The MTT test results showed that the greatest cell viability rate was in the carp nHA scaffolds after 10 days (146.08%). Moreover, the AR staining indicated the formation of mineralized nodules caused by the scaffolds in all groups. However, the mineralization seemed to be superior in human, and carp extracted groups. Furthermore, *in vivo* in all three groups bone repair occurred at the critical-size lesion sites, while scaffolds biodegradation was also observed. The scaffolds made up of carp and human nHA exhibited the highest rate of ossification and maturation of bone tissue among different scaffolds after 8 weeks. The rate of tissue response to these scaffolds was higher than the scaffolds made of commercial nHA after 4 and 8 weeks, postoperatively.

Conclusion: The carp extracted nHA scaffolds perform comparable to human extracted nHA, and may be used for clinical applications.

*Corresponding author: Marjan Bahraminasab, Emails: m.bahraminasab@semums.ac.ir; m.bahraminasab@yahoo.com

Introduction

Large bony defects and critical-size injuries, which will not heal during the patient life given the extent of damage that the body can repair, are some of the reasons for developing bone tissue engineering (TE) strategies.[1] Autografting and allografting are traditional biological methods of bone defect management. However, the defect size and the host bed viability, limit their application. Moreover, because of the unpredictable bone erosion, the new bone volume preservation can cause a problem.[2,3] The substitutes provided by tissue engineering may well restore or improve tissue function. The 3D scaffolds, as TE substitutes, establish a favorable environment to induce tissue formation, supporting growth and differentiation of cells and finally, regenerated tissue deposition.[4] The bone scaffolds should be biocompatible, osteoconductive, and osteoinductive.[5,6] Moreover, an ideal scaffold should have open pores with interconnectivity in the structure, allowing nutrients to penetrate the scaffold *in vitro* and produce vascularization *in vivo*.[7,8] Ultimately, the scaffolds should degrade at a reasonable rate matching the tissue formation rate.[9]

Hydroxyapatite (HA), the most abundant mineral in bone structure, is a popular biomaterial for bone regeneration. HA exhibits superb bioactivity, relatively suitable mechanical characteristics, and favorable biological performance. However, the properties of HA and its constructs are dependent on its particle size.[10] Nano HA (nHA) crystals have unique physicochemical properties compared to micron-size HA particles, including high surface area, high solubility, great surface energy, and high biological activity. These features make nHA highly attractive in bone replacement and reconstruction.[5] For example, the biocompatibility and cytotoxicity of the nHA/polyamide (PA) composite scaffolds in direct contact with mesenchymal stem cells (MSCs) were evaluated. In addition, the *in vivo* effects such as biocompatibility and osteogenesis in animal experiments were studied. The scaffold with 70% porosity exerted no negative effect on the MSCs growth, proliferation and osteoblastic differentiation, resulting in healing of critical-size defects of the rabbit mandible.[11] Furthermore, human fetal osteoblasts were cultured on chitosan/nano-hydroxyapatite porous scaffolds, which showed increased osteocalcin production on these composite scaffolds.[12]

The HA can be extracted from natural sources and ground to nano size. Natural sources provide advantages of biocompatibility and environment friendly.[13,14] For example, HA extraction from fish bone wastes is cost-effective with easy manufacturing protocols, which can lessen the bone repair or replacement costs.[15,16] It has been shown that the world fish production, already, has exceeded 170 million tons/year, which produces 40-80% waste, unusably discarded, as stated by the Food and Agriculture Organization of the United Nations (FAO-2016).[15] The lack of no commercially application available for the use of these residues leads to pile up landfill and ends up with severe health problems.[17] On the other hand, human extracted HA from cadaver is limited and very expensive, and requires many ethical approvals. Therefore, it is worthy to find a substitute with comparable biocompatibility and bone repair ability to that of human extracted HA, and at the same time help in waste management and environment.

To the authors' knowledge, HA extracted from carp fish has not yet been investigated for its biocompatibility and bone repair ability. Therefore, herein, the biological efficiency of scaffolds made from carp extracted nHA was investigated and compared with that of human extracted nHA by *in vitro* and *in vivo* experiments. First, the nHA powders were synthesized from human extracted, and carp extracted HA. Subsequently, porous nHA scaffolds were prepared and examined for their physicochemical, structural, and mechanical properties. Furthermore, their cytotoxicity and osteogenic differentiation *in vitro* and bone regeneration ability in repairing critical-size defects *in vivo* were also assessed.

Materials and Methods

Synthesis of HA powder from carp bone waste

The HA powder was synthesized based on the previous study[18]; briefly, the carp bones were boiled in water for about 90 minutes to remove the fat. They were then exposed to the air to dry completely. Then, 8g of the dried bones was ground in a mortar and put in an electric furnace at 700 °C for 5 hours to produce hydroxyapatite.[18]

Providing commercial & human extracted HA powders

Human and commercial powders were purchased from Iranian Tissue Product Company (Tehran, Iran) and APATECH Company (Pardis Pajoohesh Fanavaran Yazd Co., Iran), respectively.

Preparation of nHA

To prepare nanoscale powders, microscopic images were, first, taken to study the initial particle dimensions of the different HA powders using field emission scanning electron microscopy (FE-SEM, MIRA3, TESCAN, Czech Republic). Since the dimensions of HA powders extracted from humans and carp were larger than 100 nm, a high-energy planetary ball mill (HEBM) with Teflon cup and tungsten ball (Nano shot-Amin Asia, Iran) was used. The HA powders extracted from carp and human bones were ground for 2 and 60 hours, respectively, at 400 rpm using a ball to powder ratio of 20:1, and a rest time of 15 minutes for a 1-hour rotation. However, after ball milling for 60 hours, the dimensions of human HA powder were not in nanoscale. Therefore, it was exposed to a thermal processing using an electric furnace at 800 °C for

1 hour. Then, the furnace door was opened at the high temperature (800 °C) to achieve finer powder particles by rapid cooling. It is noteworthy that the commercial hydroxyapatite powder had nano dimensions. The FE-SEM images were prepared at the different stages of grounding to ensure accurate conversion of particle dimensions into nano size. Image J software was used to examine the particle size.

Characterization of powders

X-ray diffraction analysis (XRD)

XRD analysis was used to determine the phases in the prepared powders. The analysis was conducted at a voltage of 35 kV and a current of 30 mA, using a Cu Kα beam and the scanning range of 10-60 degrees (Bruker, D8-advance).

Fourier transform infrared spectroscopy (FTIR)

FTIR was conducted using Bruker-Tensor 27 IR, USA to determine the chemical bonds in the powders. The KBr powder was used through a standard method to perform the test. The spectrum with a resolution of 2 cm^{-1} was obtained in the frequency range of 4000-400 cm^{-1}.

Scanning electron microscopy (SEM) imaging

First, the HA powders were placed on the foil and covered by a thin layer of gold to perform SEM (MIRA3, TESCAN) imaging. The images obtained were utilized to measure the dimensions of the powder particles using ImageJ software.

Measurement of calcium to phosphate ratio

Energy-dispersive X-ray spectroscopy (EDS) was performed on the powders (TESCAN MIRA3 LMU) to determine the ratio of calcium to phosphorus (by dividing the atomic percentage of Ca into P). The EDS elemental analysis was performed at 5 points on each powder.

Scaffold Fabrication

To fabricate the scaffolds, the powders were mixed with a biner and a sintering process was used.[19,20] First, 5% polyvinyl alcohol (PVA) solution was prepared to fabricate the disc-shaped scaffolds from the commercial and carp powders, while for making the scaffolds from human extracted powder 10% PVA solution was used to achieve similar porosity. PVA acts as a binder and causes the powder particles to be attached to each other. The 5% PVA and 10% PVA solutions were prepared by mixing 5 g of the PVA powder with 95 mL of distilled water, and 10 g of the PVA powder with 90 mL of distilled water, respectively, using a magnetic stirrer at 70°C with a rotation speed of 300 rpm. Then, 0.3 g of the nHA powder was mixed with 8 drops of 5% PVA solution in the case of commercial and carp-derived powders, and 4 drops of 10% PVA solution in the case of human-derived powder. The mixture was then compressed into a plastic mold made by a 3D printer. The samples were, finally, sintered in an electric furnace for 1 hour at 300 °C (to remove PVA) followed by 1 hour at 1100 °C, after their removal from the mold.

Scaffold characterization, porosity measurement, and morphology analysis

XRD analysis

Since the scaffolds were sintered in the oven at high temperatures (1100 °C), there was a possibility for the phase change; therefore, XRD analysis was used again to determine the phases in the prepared scaffolds. The analysis was conducted at a voltage of 35 kV and a current of 30 mA, using a Cu Kα beam and the scanning range of 10-60 degrees (Bruker, D8-advance).

SEM imaging

The scaffolds were initially coated with a thin layer of gold for imaging, which was performed in secondary electron mode at a voltage of 15 kV (Philips XL30, Netherland).

Measurement of porosity percentage and density

To determine the porosity, first, the average of diameter and height of each scaffold were measured by a caliper. Furthermore, the mass of each sample was then measured by a sensitive digital scale to calculate the density using equation 1.

$$d = \frac{m}{\pi r^2 h} \quad (1)$$

Where, *d, m, r*, and *h* represent the density, the mass, the average radius, and the average height of each scaffold, respectively.

Finally, the porosity of each scaffold was calculated using equation 2.[21-23]

$$P\% = 100 \times \left(1 - \frac{d}{p}\right) \quad (2)$$

In the above equation, P indicates the porosity and p is the density of hydroxyapatite (3200 kg/m^3).

Evaluation of biodegradability in vitro

The in vitro biodegradability of the scaffolds made by different nHA powders was evaluated by weight measurements before and after soaking into the PBS solution up to 41 days, and the degradation ratio (%) was calculated using equation 3.

$$Degradation\ ratio(\%) = \frac{w_0 - w_t}{w_0} \times 100 \quad (3)$$

In this equation w_0 signifies the weight of the scaffolds before immersion in PBS and w_t denotes the scaffold weight after immersion at different time points.

Assessment of mechanical properties

Compression tests were conducted to evaluate the mechanical properties of the scaffolds using a Universal Testing Machine (UTM, Santam Co., Iran). The loading

rate was 1 mm/min to a compressive strain of 80%. The stress–strain (σ–ε) curves of the scaffolds were drawn by dividing the force to cross-sectional area (to obtain σ), and the displacement to initial length (to obtain ε). The compressive modulus (E) was then calculated as the curve slope of the initial linear region and the ultimate compressive strength (UCS) was identified as the maximum stress on the curve.

Scaffold sterilization and extract medium

The scaffolds prepared from the powder with an average diameter of 7.6 mm and height of 3-4 mm, were washed with 70% alcohol, wrapped in foil and sterilized at 100 °C for 1 hour. After sterilization, two samples from each group were immersed in 2.5 mL culture medium in a 24-well plate for 3 days. The scaffolds were then removed and the culture media (extracts) were used for the cellular tests.

Cell culture

First, the MC3T3 cell line (C57BL/6 mouse skull pre-osteoblast supplied by Sigma Aldrich, Sweden) was cultured in Dulbecco's Modified Eagle's medium (DMEM) medium.[24] To prepare the complete medium, 10% fetal bovine serum (FBS) supplied by Gibco Life Technologies, 100 units of penicillin, 100 µg/mL streptomycin , and 2 mM glutamine supplied by Gibco Life Technologies were added to the culture medium. The cells were then cultured in an incubator at a temperature of 37 °C, 5% CO_2, and 95% humidity. An inverted light microscope was used to evaluate the quality of the cultured cells. For routine passages, the culture medium was discarded, and PBS solution was used to wash the cells, followed by trypsinization, centrifugation, and finally transfer of the cells to a new flask with a fresh culture medium.

MTT assay

Biocompatibility was assessed at 3, 5, and 10 days for the scaffolds made from carp extracted, human extracted, and commercial nano-hydroxyapatite powders. Furthermore, a control group was also examined, where the cells were cultured in complete culture medium and not exposed to the scaffold extract medium. The MC3T3-E1 cells were cultured at a rate of 5000 cells per well in a 96-well plate to reach 80% confluence in 24 hours. The culture extract (scaffold culture supernatant) was added to the cells, which were then incubated for 3, 5, and 10 days. The cell viability at these intervals was assessed by the MTT (Cell Growth Determination Kit, Sigma Life Science) cell proliferation measurement kit according to company guidelines. Overall, the culture medium in each well was replaced by 100 µL of incomplete culture medium, followed by adding 10 µL of MTT solution to each well and incubating for 4 hours at 37 °C. At the end of the incubation, 100 µL of 0.04 N hydrochloric acid in isopropyl alcohol was added to each well, and the formed insoluble formazan was dissolved by pipetting up and down. Finally, the absorbance was measured at 570 nm by ELISA microplate Reader (Synergy H1 Hybrid Multi-Mode Microplate Reader, BioTek, USA) and viability rate (%) was obtained according to equation 4.

$$Viability\,ratio(\%) = \frac{A_{sample}}{A_{control}} \times 100 \quad (4)$$

Where A_{sample} and $A_{control}$ are the absorbances of the studying materials and the control (cells alone with on scaffold extract), respectively.

Alizarin red assay

Alizarin red (AR) staining, was used to assess calcium deposition by cells after 7 days of incubation in an osteogenic medium. First, 5×10^3 MC3T3-E1 cells per well were cultured in a 24-well plate and it was kept in an incubator at 37 °C in CO_2 and 95% humidity. After forming a cell monolayer (24 h), the scaffold media (extracts) along with osteogenic materials (50 µg/mL ascorbic acid, and 10mM β-glycerophosphate) (Sigma-Aldrich, USA)) were added. At the end of the incubation time, the cells were fixed with paraformaldehyde (4 v/v%) for 15 min at 4 °C, then washed with PBS and stained with 1% (w/v) AR for 40 min at room temperature in dark conditions. Lastly, the AR stain was removed from the wells, and washing with PBS was done several times to remove unreacted AR stain. Finally, the samples were observed under a loop microscope.

Animals

The animal study was carried out according to National Institutes of Health guide for care and use of laboratory animals. All procedures were approved by the ethics committee of Semnan University of Medical Sciences (permit number: IR.SEMUMS.REC.1398.273). The present study used adult female rats with a mean weight of 230 (±20) g.

The rats were kept in standard conditions in an animal house with free access to water and food. The animals (rats) were randomly divided into 4 groups, including 3 experimental groups (n = 30, 10 animals in each group) and one control group (n = 4). Table 1 presents the details of the studied groups.

Table 1. *In vivo* experimental groups by scaffold type and follow-up period

No.	Group	Time (wk)	Number of animals
1	Cavity without scaffold (Control)	4 8	4
2	Carp hydroxyapatite scaffold	4 8	10
3	Human hydroxyapatite scaffold	4 8	10
4	Commercial hydroxyapatite scaffold	4 8	10

Implantation

The scaffolds were implanted in critical-size defects (8 mm in diameter) of the calvarium of rats. After anesthesia using ketamine and xylazine (volume ratio of 8:2 at 1 mL/kg),[25] the animal head was fixed in a stereotaxic frame. Using a scalpel, an approximately 1.5 cm incision to the periosteum over the scalp from the nasal bone to just caudal to the middle sagittal crest or bregma was deepened. Then, by laterally counter-traction, the calvarium was visualized, and the periosteum covering it was divided down the sagittal midline with the scalpel, and pushed laterally. Manually, the soft tissues were retracted and the underlying bone was exposed. The site was irrigated with sterile normal saline. Using a surgical drill and an appropriate trephine, the defect was formed on the calvarium (craniotomy). The trephine and calvarium were irrigated with sterile normal saline to lessen the influence of generated heat during drilling. Care was taken not to penetrate the calvarium too deeply. Trephination, to prevent dura or brain injury, continued with a controlled downward pressure. During this process, the trephine was withdrawn and the margins of defect were evaluated. After adequate drilling, using an elevator blade into the margin of defect circumferentially around the defect, with slight pressure the defect bone was lifted gently with the elevator. Finally, the elevator blade was carefully slid under the freed calvarium and swept backwards and forwards, releasing the dura from the bone underside. The implant was placed at the site of the defect, and the scalp was sutured (Fig. 1a). All surgical operations were carried out by a single person using the same drill and specific drilling speed to minimize the subjective bias. Furthermore, the operations were conducted in different days (4-5 animals each day) having at least one implantation for each group. The order of the group implantation was randomly chosen in each day.

After completion of the surgery, the head was carefully cleaned with saline or diluted hydrogen peroxide. The rat was transferred to a warmed incubator. After regaining full consciousness for about 2 hours and completion of observation, the rat was transferred to normal husbandry cage and housed individually until tissue harvesting.

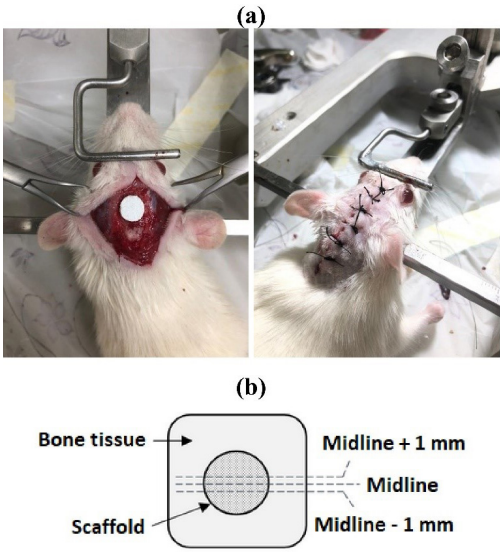

Fig. 1. (a) the scaffold implantation into the critical-size lesion (8 mm in diameter) created in the rat skull, and (b) schematic of the harvested tissue and the region of study.

Euthanasia and implant harvest

To harvest the tissue, 4 and 8 weeks postoperatively, the rats were placed into the induction chamber and euthanized using 2 L/min flow of carbon dioxide for 5 min or until breathing ceased. To ensure death, an animal guillotine was used. Finally, a section of the cranium containing the implant was removed.

Histological analysis

The harvested tissues, after fixation in 10% neutral buffered formalin solution and decalcification processing in 10% formic acid solution, were dehydrated in serially increasing ethanol. The dehydrated samples were then embedded in paraffin, cut into 5mm thick cross sections and stained with hematoxylin and eosin.[9] The analyzed area in histology is schematically shown in Fig. 1b.

Results

Characterization of different types of nano hydroxyapatite powders

Existing phases

The phase analysis of the calcined carp powder at 700 °C, human extracted powder before and after heat treatment at 800 °C and the commercial nHA powder was performed by the XRD technique. Fig. 2a shows the XRD spectra of the HA powders. The XRD spectra of calcined carp powder and human extracted powder before and after heat treatment well matched with those of HA (reference cards of 24-0033, 01-1008, and 34-0010 for carp, human and human heat-treated, correspondingly). Traces of other calcium phosphate impurities were not found. In the HA powders of carp and human heat-treated powders, the HA main peaks associated with crystalline planes of (211), (112) and (300) diffracted at 2θ about 31.8°, 32.2°, and 32.9°, respectively. These peaks have been reported in the prior studies on HA synthesis.[26,27] Furthermore, these powders exhibited well crystallized structures because the baselines in their XRD diffractograms are straight and the peaks are sharp and narrow. The XRD diffraction of human extracted powder before heat treatment, however, showed less sharpness in the peaks and has slightly more noisy background compared to the other HA powders. This implies that the structure was amorphous before heat treatment, and it became crystalline after heat treatment. As it can be seen in Fig. 2a, the pattern associated with commercial powder showed the peaks related to HA, Ca-

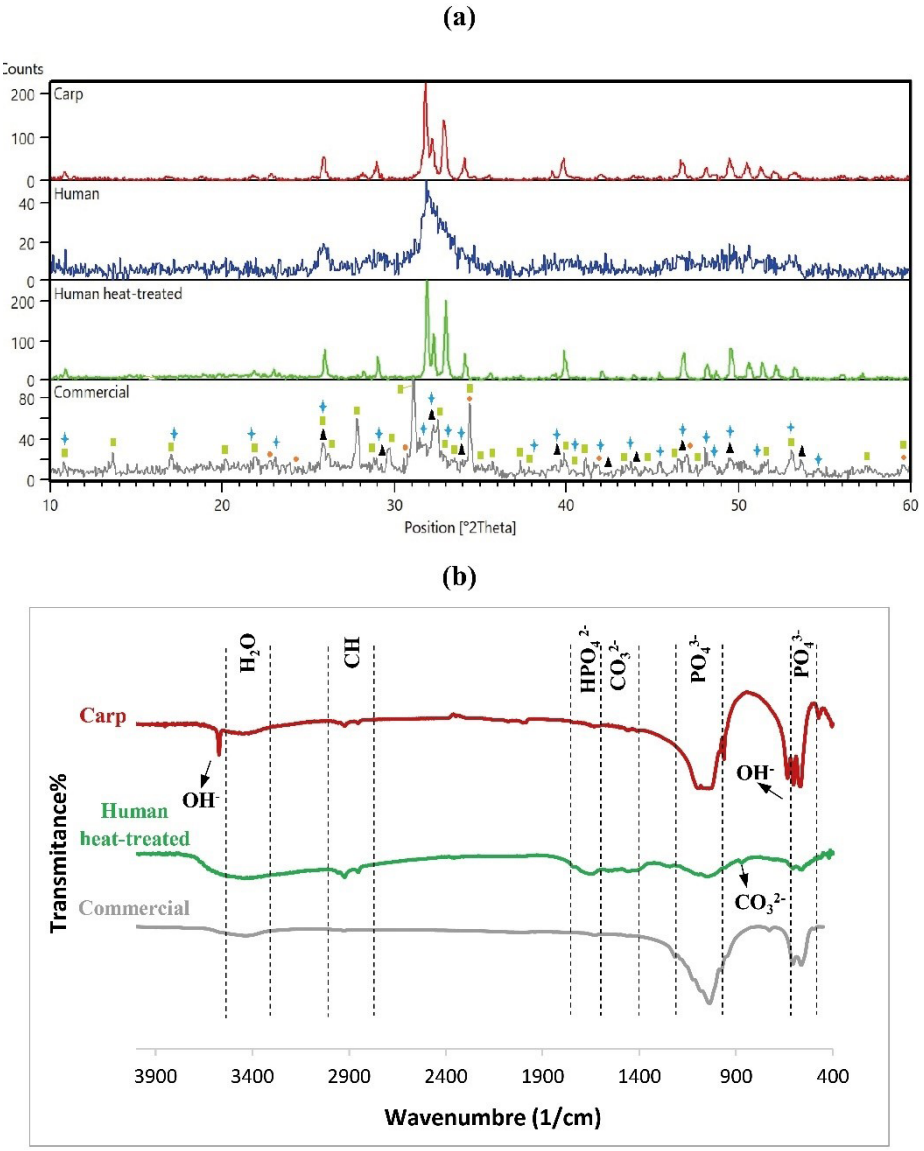

Fig. 2. Phases and chemical bonds of different HA powders (a) XRD spectra (triangles, circles, rectangles and stars are indicatives of HA, alpha tricalcium phosphate, whitlockite, and Ca-deficient HA, respectively), and (b) FTIR patterns.

deficient HA (calcium hydrogen phosphate hydroxide ($Ca_9HPO_4(PO_4)_5OH$)), alpha tricalcium phosphate (α-$Ca_3(PO_4)_2$), and whitlockite ($Ca_3(PO_4)_2$). These phases are shown by triangles (HA), circles (alpha tricalcium phosphate), rectangles (whitlockite) and stars (Ca-deficient HA) in Fig. 2, which are in agreement with previous research.[16,28-34] The reference cards related to HA, Ca-deficient HA, alpha tricalcium phosphate, and whitlockite are 01-1008, 46-0905, 03-0681, and 09-0169, respectively.

Chemical bonds

Fig. 2b shows the FTIR spectra of hydroxyapatite powder extracted from carp and human, and commercial HA. In the FTIR spectra of hydroxyapatite powder, there should be compounds such as phosphate (PO_4^{3-}), carbonate (CO_3^{2-}), and hydroxyl (OH^-) ions. The P-O and O-H functional groups observed in all hydroxyapatite powders indicated the formation or presence of hydroxyapatite. In addition, the functional group of CO_3^{2-} was also identified in the HA powders extracted from carp and humans, indicating the formation of carbonate apatite. This is probably as a result of the replacement of OH^- and PO_4^{3-} with CO_3^{2-} in the hydroxyapatite crystal structures, possibly from reacting with CO_2 in the air. The presence of carbonate in hydroxyapatite is not a concern but actually an advantage. Carbonate can act as natural carbonate in bone hydroxyapatite, and improve bone biocompatibility and osteoconductivity.[35-37] The FTIR bands in 632 cm^{-1} and 3572 cm^{-1} belong to hydroxyl groups,[16,38] and phosphate peaks were identified in the range of 1100-1030, and at 962, 603, and 473 cm^{-1} in the hydroxyapatite powder extracted from carp.[39] The phosphate bands were also found in human extracted (559, 607, 1047, and 1093 cm^{-1}) and commercial (497, 563, 606, 978, and 1037 cm^{-1})

HA powders. The characteristic peaks, usually in the range 3412-3440 cm^{-1}, are water molecules,[40] observed in all hydroxyapatite samples. The weak carbonate-related bands appeared in carp extracted hydroxyapatite nearly at a range of 1500-1400 cm^{-1}.[26,27,41,42] These bonds were more evident in human extracted hydroxyapatite, but were not detectable in the commercial hydroxyapatite spectrum. In addition, another peak related to the carbonate group can be detected at around 873 cm^{-1}, which was only observed in the FTIR spectra of human extracted hydroxyapatite. The band appeared in carp extracted hydroxyapatite at 1640 cm^{-1} is related to hydrogen phosphate (HPO_4^{2-}).[43] This peak was also identified in human extracted (1655 cm^{-1}) and commercial (1629 cm^{-1}) HA. The FTIR peaks detected at the range of 2800-3000 cm^{-1} are related to Alkane,[16,44,45] which were only observed in human and carp extracted hydroxyapatite powders with higher intensity in the former.

Morphology

Fig. 3 shows SEM images of different hydroxyapatite powder particles. Fig. 3a indicates the SEM images of carp extracted HA powder where the powder morphology is

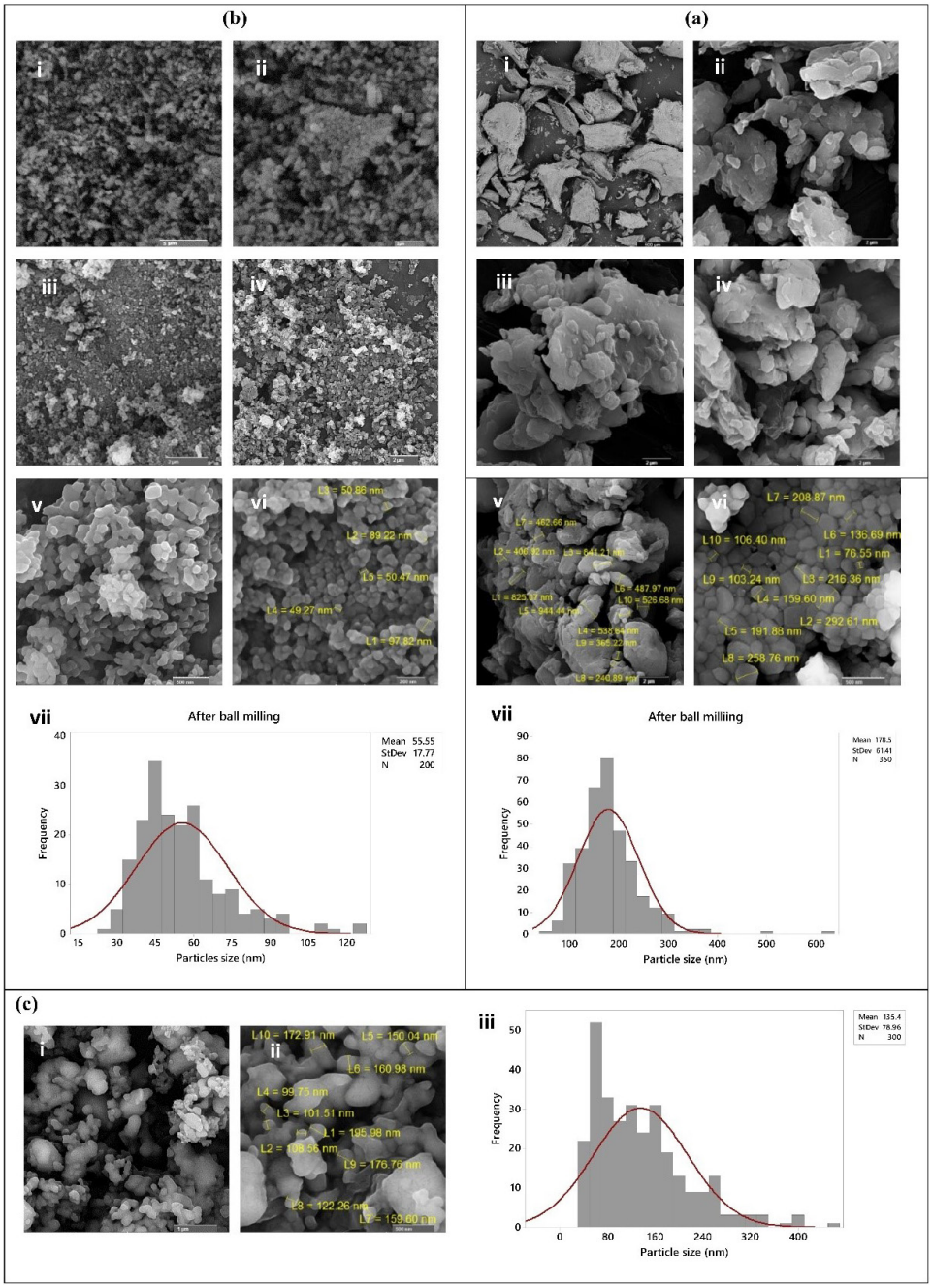

Fig. 3. SEM images and particle size distribution of (a) Carp extracted nHA powder; (i) and (ii) before ball milling, (iii-vi) after grinding for 2 hours, and (vii) histogram of particle size, (b) Human extracted nHA powder; (i) before ball milling, (ii) 4 hours after ball milling, (iii) 10 hours after ball milling, (iv) 30 hours after ball milling, (v) 60 hours after ball milling, (vi) after thermal processing at 800°C for 1 hour, and (vii) histogram of particle size, and (c) Commercial nHA powder; (i and ii) as provided particles at 2 different magnifications, and (iii) histogram of particle size.

shown before ball milling at two different magnifications (Fig. 3a (i and ii)). The ground HA powder after two hours of ball milling (Figs. 3a (iii-vi)) was identified to become completely fine and into nano size. The particle size and distribution were 55.55 ± 17.77 nm and 22.5-127.5 nm, respectively (Figs. 3a (vii)). Fig. 3b (i-vi) shows the conversion of human powder particles from micro to nano size by the planetary ball mill and thermal processing. As it is shown in Fig. 3b (i), the human extracted powder had a very large particle size with a completely irregular morphology before grinding with a planetary ball mill. After ball milling of the powder for 4 (Fig. 3b (ii)) and 10 (Fig. 3b (iii)) hours, the size of particles decreased, but a mixture of fine and relatively coarse particles was observed in the powder. After ball milling of the human extracted HA powder for 30 (Fig. 3b (iv)) and 60 (Fig. 3b (v)) hours, the powder particles became finer and smaller, but heterogeneity in the size of the powder particles was still evident. Furthermore, as an increase in the particle grinding time from 30 to 60 hours did not exert any significant effects on the reduction of the powder particle size. Therefore, thermal processing was used to further grind the powder. Thermal processing at 800°C for 1 hour was conducted with rapid cooling, reducing the powder size (Fig. 3b (vi)) and homogenizing the particles. The particle size and distribution were 178.5 ± 61.41 nm and 37.5-387.5 nm, respectively, after thermal processing (Fig. 3b (vii)).

As mentioned in the Methods section, the commercial powder was initially purchased in nanoscale, as it can be seen in SEM images (Fig. 3c (i and ii)). The particle size and distribution were 135.4 ± 78.96 nm and 30.0-410.0 nm, respectively (Fig. 3c (iii)).

Calcium to phosphorus ratio

The results of EDS analysis identified the calcium to phosphorus (Ca/P) ratio (Table 2). The highest Ca/P ratio was related to commercial nHA, followed by the carp extracted and human extracted (before heat treatment) nano-hydroxyapatite powders, respectively. The Ca/P ratio increased after heat treatment in the human extracted nHA.

Characteristics of nHA porous scaffolds

Existing phases

Fig. 4 shows the XRD pattern of the porous scaffolds sintered at 1100 °C. The peaks appeared for scaffolds of carp and human extracted nHA powders represented the same characteristic peaks as those of HA powders (raw materials) and are in agreement with previous studies.[46-52] The XRD peaks for carp extracted nHA scaffolds conformed to the reference card of 03-0690. The diffractogram of human extracted nHA scaffolds also matched with reference cards of 34-0010 and 24-0033. Accordingly, no phase changes occurred following sintering in the electric furnace at 1100 °C. However, in the scaffold made from commercial powder, whitlockite (reference card of 09-0169) and beta tricalcium phosphate (reference card of 03-0690) were observed, implying that whitlockite was not transformed, while other calcium phosphates including HA, Ca-deficient HA, and alpha tricalcium phosphate were all transformed to beta

Table 2. Calcium to phosphorus mean ratio in carp extracted, commercial, and human extracted nanohydroxyapatite powders

Type of powder	Average atomic ratio of calcium to phosphorus
Carp	1.56 ± 0.01
Human (before heat treatment)	0.77 ± 0.35
Human (after heat treatment)	2.58 ± 0.01
Commercial	1.78 ± 0.04

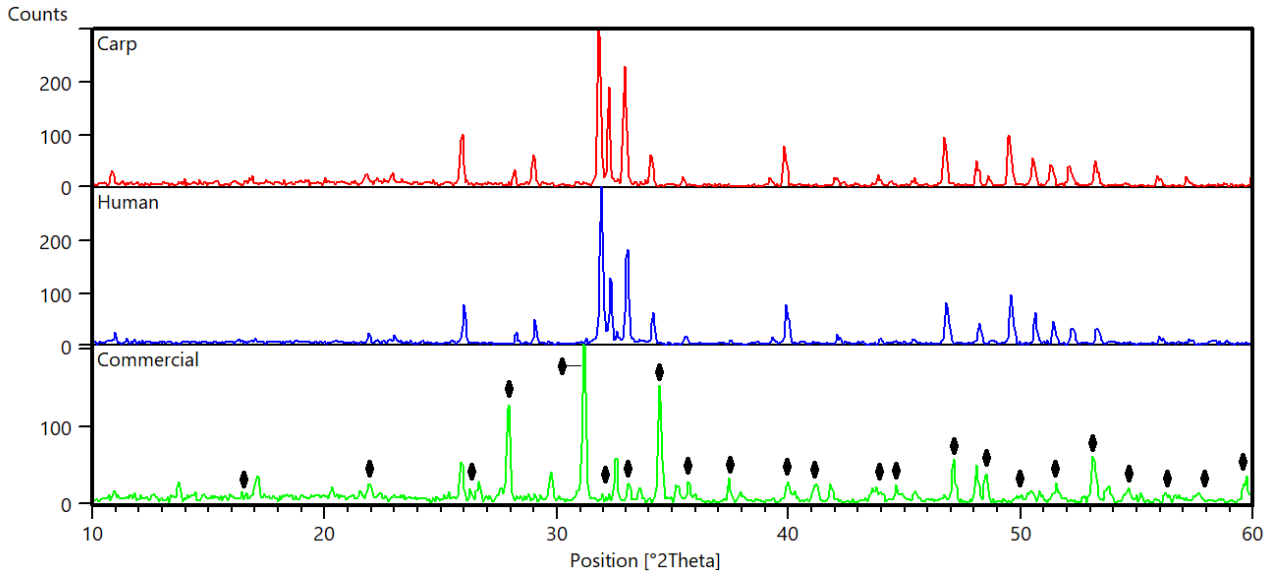

Fig. 4. XRD patterns of different nHA scaffolds. The peaks related to the beta-tricalcium are shown with diamonds.

tricalcium phosphate. The peaks associated with beta tricalcium phosphate are indicated by diamonds in Fig. 4 and are in agreement with previously reported data.[53-55]

Surface morphology

Fig. 5 shows the SEM images of the surfaces of nano-hydroxyapatite scaffolds. As shown in the figure, the scaffolds of all three groups became completely porous after sintering. It has been indicated that the rough surface and porosity contribute to the superior biological performance of the scaffold and aid in new bone growth.[56,57] As it is evident, the size of the pores in the commercial scaffold was slightly larger than those composed of carp and human extracted nHA scaffolds.

Physical properties

According to the findings in Table 3, the scaffolds composed of carp extracted nHA had the highest density, followed by those composed of human extracted, and commercial nano-hydroxyapatite powders, respectively.

Table 3. Physical properties (density, and porosity percentage and pore size) in different scaffolds

Type of scaffold	Pore size (μm)	Porosity (%)	Density (kg/m³)
Carp	6.91 ± 6.02	60.68 ± 2.36	1258.22 ± 75.82
Human	2.38 ± 4.78	61.38 ± 2.47	1235.6 ± 79.26
Commercial	14.66 ± 13.07	63.27 ± 1.24	1172.93 ± 38.47

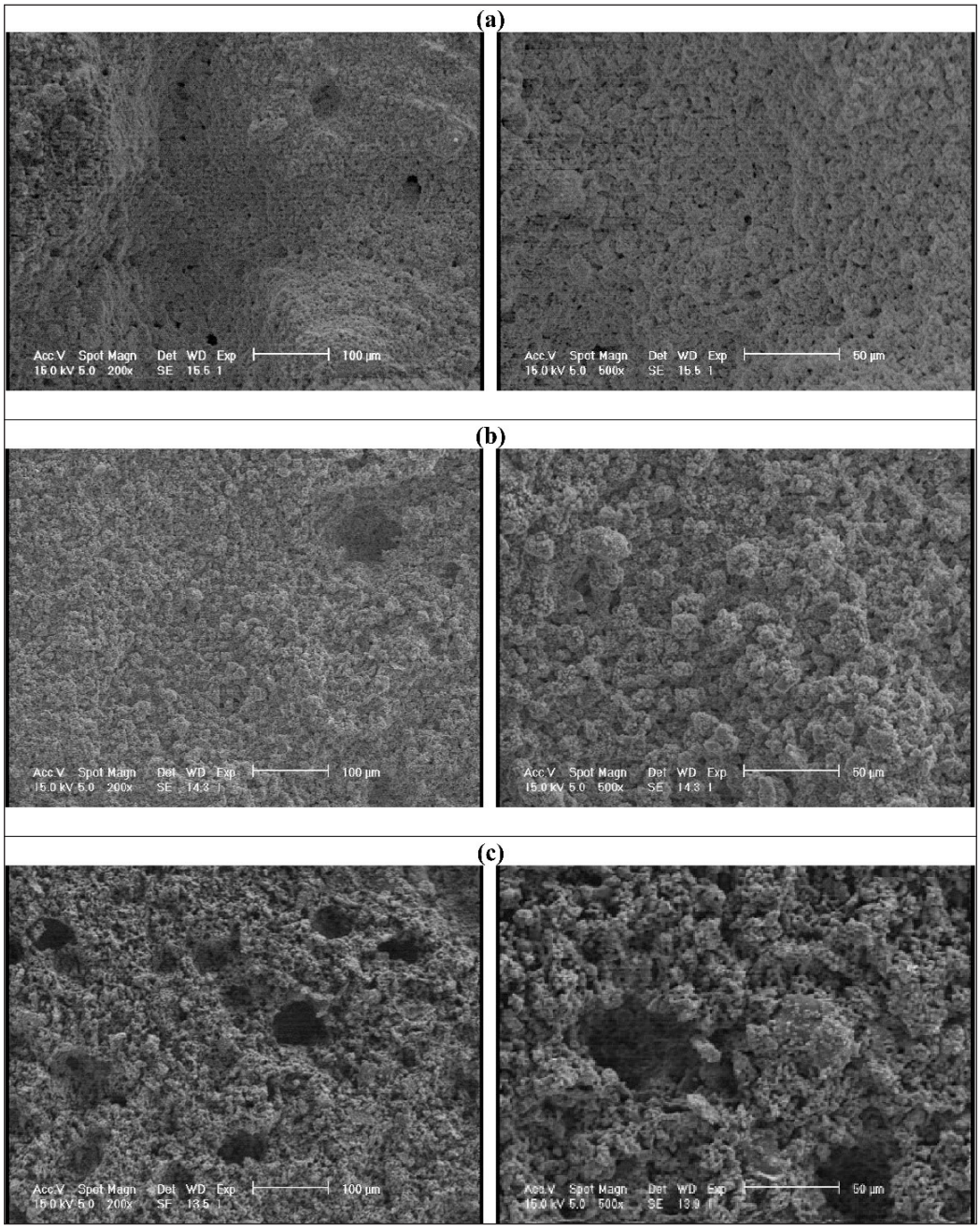

Fig. 5. SEM images of the surfaces of nHA scaffolds fabricated with powders: (a) extracted from carp bone, (b) extracted from human bone, and (c) commercial

However, the highest mean percentage of porosity among the scaffolds of these three powders was related to the commercial group. This was followed by human extracted, and carp extracted groups, respectively. However, the difference between the mean percentage of porosity and density among the groups was insignificant. Moreover, the commercial group had the largest mean pore size. The carp and human extracted nHA scaffolds had smaller pores of approximately similar size.

In vitro biodegradability of scaffolds

The *in vitro* biodegradability was accomplished by soaking the scaffolds in PBS for 41 days at 37 ± 0.5 °C using a thermostatic oven. The weight changes of the scaffolds were calculated and the biodegradability ratio was obtained based on equation 3. The biodegradability profiles are shown in Fig. 6a. As it can be seen the scaffolds made up of human extracted nano-hydroxyapatite powder revealed a faster degradation rate, while the other two groups had slower degradability. The scaffolds made up of carp extracted and commercial HA started to degrade at day 24 and day 37, respectively. The means of degradability% were 16.75%, 1.13%, and 0.64%, in respect, for human, carp and commercial groups at day 41.

Mechanical properties of scaffolds

The mechanical strength and stiffness of the scaffolds were measured and the results are presented in Fig. 6b. The results indicated that the scaffolds made up of human extracted nano-hydroxyapatite powder had the lowest UCS (3.13 KPa) and E (37.37 KPa). Therefore, these scaffolds were very soft. However, those fabricated by carp extracted and commercial nano-powders showed higher strength, but comparable to each other (17.14 and 19.01 Kpa, respectively). The elastic moduli were also higher in carp and commercial groups, with greatest value obtained for the scaffolds made up of carp extracted nano-hydroxyapatite powder (251.79 Kpa). These results are in agreement with the findings of our biodegradability test where the scaffolds in human group degraded more rapidly in comparison with carp and commercial groups.

Cytotoxicity of nHA scaffolds

The MC3T3-E1 cell viability was assessed by MTT assay after 3, 5, and 10 days of culture. Fig. 7a shows the cell viability (in percentage). As shown in this figure, the viability percentage was high in the initial exposure to the studied materials (111.3, 100.8 and 116.3 for carp, human and commercial groups, respectively). The commercial group exhibited the highest mean viability percentage at day 3 compared to other time points. The same trend was observed for the viability rate after 5 days. The highest viability percentage was shown in the scaffolds composed of carp extracted nHA (146%) after 10 days, which was the highest value in all groups at different time points. Analysis of variance showed that time and material*time variables exerted significant effects on the rate of viability (P-values of 0.002 and 0.039, respectively). Furthermore, Tukey analysis as a pairwise comparison test is presented in Fig. 7a. The groups that do not share a letter are statistically significant.

Matrix Mineralization using Alizarin Red

Fig. 7b displays the calcium deposition and mineralization of MC3T3-E1 cells in the osteogenic cell culture medium at day 7. The results of AR staining indicated the formation of mineralized nodules caused by the scaffolds in all groups. However, the intensity of red color was higher in human, and carp extracted groups.

Histology

The ability of the scaffolds to allow new bone formation in critical-size calvarial lesions was examined by hematoxylin and eosin staining (Fig. 8).

The bone regeneration in different groups 4 and 8 weeks postoperatively

Fig. 8a indicates the regeneration of bone in the defect sites after 4 weeks in rats of different groups. Bone regeneration was completely done in all three groups of carp, human, and commercial scaffolds, and there were no defects without new bone formation. The osteocytes,

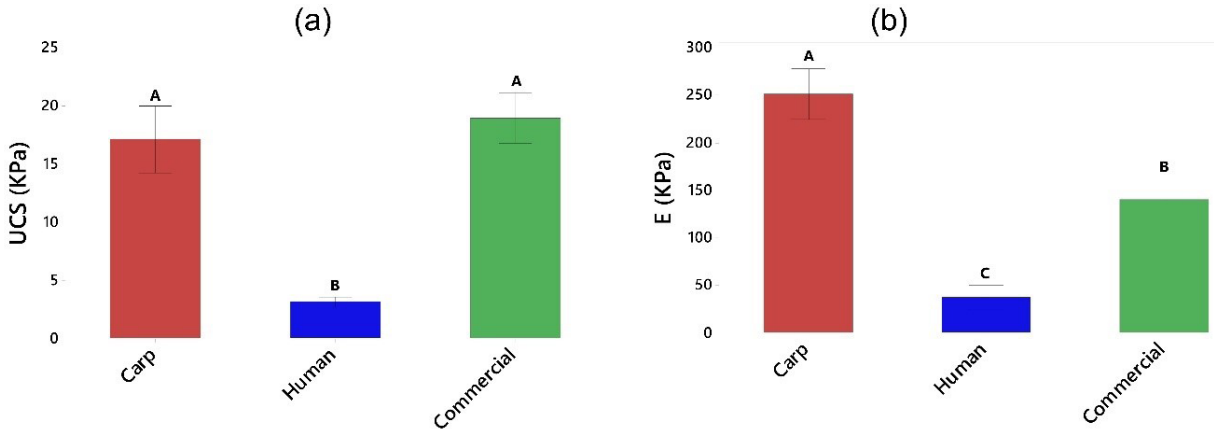

Fig. 6. (a) Biodegradability, and (b) Mechanical properties of the scaffolds. The groups (bars) that do not share a letter are statistically significant.

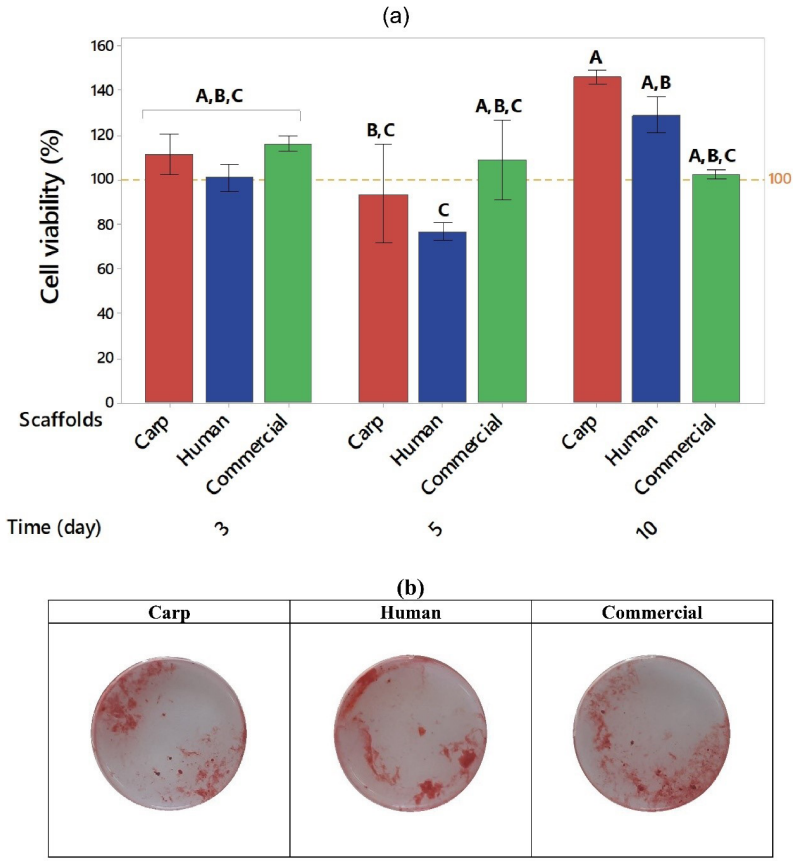

Fig. 7. (a) Mean viability rate (%) in carp, human, and commercial groups after 3, 5, and 10 days, and (b) Cell mineralization after 7 days, stained by AR. The groups (bars) that do not share a letter are statistically significant.

arteries, and bone tissue were clearly visible. Another noteworthy point was the complete formation of mature bone tissue and the observation of bone marrow and blood vessels generation in human extracted nHA scaffolds. Bone islands were observed in addition to bone mature tissues in carp and commercial groups. Concerning the degree of inflammation, histological examination showed no neutrophils or lymphocytes, confirming the high biocompatibility of the scaffolds in all three groups. Furthermore, there was no tissue formation in the untreated defect groups 4 weeks postoperatively. Another important point was that, by visual inspection of the implanted area, it was observed that the scaffolds in all groups were biodegraded, with a much lesser rate of biodegradation observed in the commercial nHA group. The in vivo biodegradation seemed to be highest in the human group, followed by the carp and commercial groups. Indeed, it appeared that the amount of remaining scaffold was the lowest in the human group.

Fig. 8b indicates the regeneration of bone after 8 weeks in the skull of the rats in different groups. The mature bone tissue was thoroughly formed and filled the defects in all three groups. The osteocytes and blood vessels were visible in all groups. Moreover, the lamellar (layered) structure of bone tissue was evident in the carp and human groups, indicating that the regenerated bone tissue was more mature in these two groups than in the commercial group. The histological observation on the inflammatory cells was similar to the results of different groups 4 weeks after surgery (no inflammatory cells were detected). Furthermore, there was no tissue formation in the untreated defect groups 8 weeks postoperatively. In addition, according to the visual inspection of the implanted area, a quite high remaining material of the scaffolds from the commercial group was still observed at the site of the lesions. However, the remnants of the scaffolds in the other groups (carp and human) were very negligible.

Qualitative comparison of bone regeneration 4 and 8 weeks after implantation

According to the morphologic comparisons of osteocytes in the two time points, the 8-week groups exhibited more elongated osteocytes and lacunae around them, indicating greater maturity of these cells. Furthermore, the bone islands changed into the integrated mature bone tissues over time in the commercial and carp groups. The lamellar structure was observed in bone tissues of the human and carp groups, indicating its greater maturity than the 4-week groups and the positive effect of time on the maturity of the regenerated bone tissue.

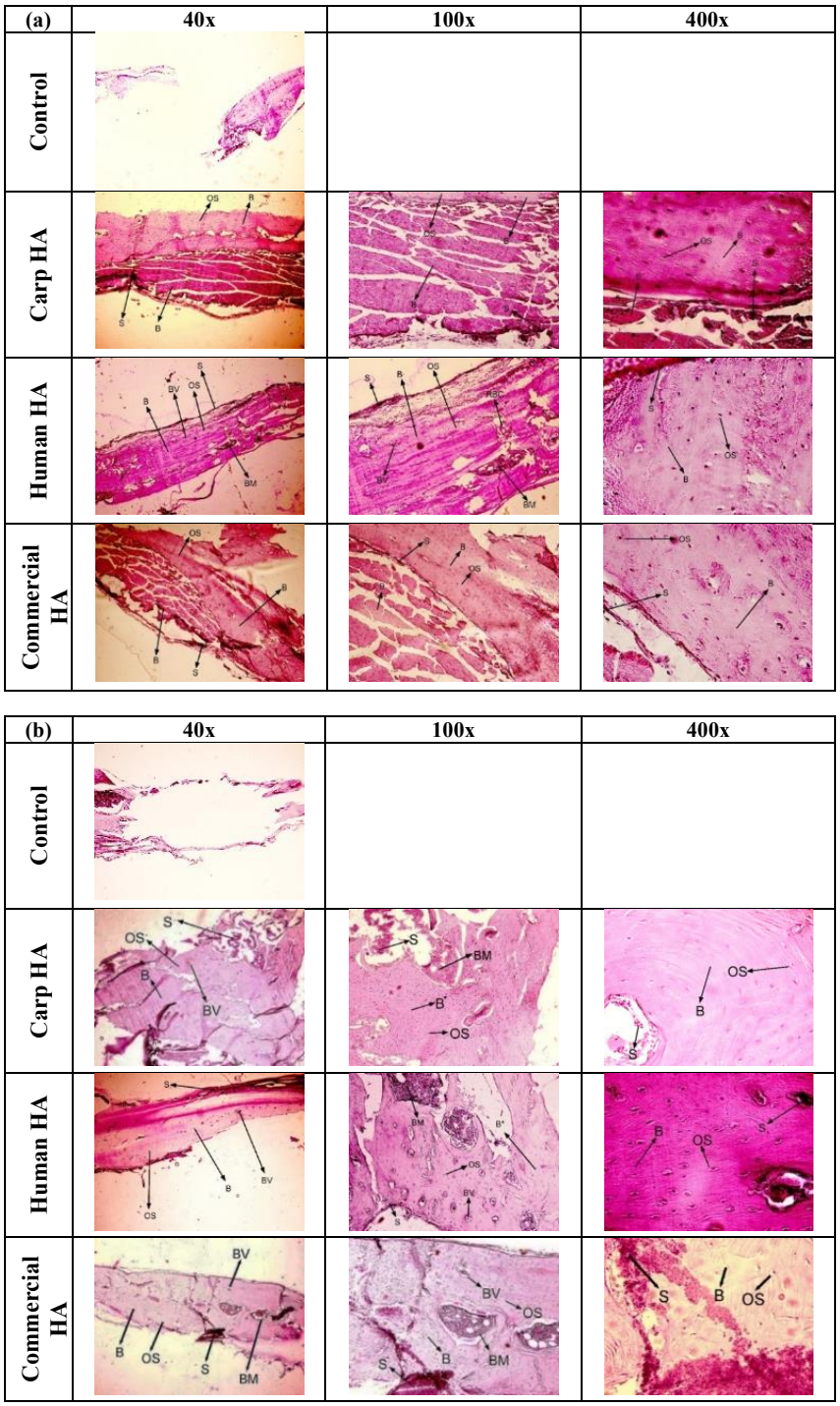

Fig. 8. H&E images in different groups after (a) 4 weeks, and (b) 8 weeks. S: Scaffold, OS: Osteocytes, BV: Blood vessels, B: Bones, BM: Bone marrow, RBC: Red blood cells.

Discussion

Nano-hydroxyapatite has been considered in the treatment of bone lesions or in the implant manufacture because of its superior biological performance (compared to the micro size), including osteointegration and new bone formation. The planetary ball mill was used in the present study to grind the carp extracted hydroxyapatite powder particles, resulting in the formation of nanoparticles after 2 hours. However, thermal processing of the powder was also required in addition to ball milling (60h) to obtain nanoparticles in the case of human extracted hydroxyapatite powder. The obtained particle sizes were 55.55 ± 17.77, 178.5 ± 61.41 and 135.4 ± 78.96 nm, respectively for carp and human extracted and commercial nHA powders. Here, the average atomic ratio of calcium to phosphorus of carp extracted nHA, human extracted nHA after heat treatment and commercial nHA were 1.56, 2.58, and 1.78, respectively. The Ca/P ratio is

important in the formation of apatite and new bone for which the molar ratio should be 0.58-2.34 (theoretically 1.67).[58] The previous EDS analyses showed that the calcium to phosphorus ratio for carp extracted hydroxyapatite was 1.65 at the temperature of 950°, very close to the results of the present study.[16] The bone scaffolds with similar porosity were prepared from three nano-powders, because it has been shown that the degree of porosity affects the biological behavior of the scaffolds and bone substitutes.[56,59] One important factor in the success of implanted scaffolds is the initial mechanical stability at the defect site, which could be provided by the rough and porous surfaces of the scaffolds (as shown in the SEM images) in all the groups studied here. The mechanical strength and stiffness of the scaffolds made up of human extracted nano-hydroxyapatite powder were the lowest. However, the scaffolds fabricated by carp extracted and commercial nano-powders showed higher strengths, and elastic moduli. The stiffest scaffolds were those built from carp extracted nano-hydroxyapatite powder. The results obtained here, are in agreement with the biodegradability findings where the scaffolds in human group degraded more rapidly in comparison with the two other groups.

According to the MTT test results in this study, the scaffolds made from all three types of nano-hydroxyapatite powders including human, carp, and commercial powders exhibited appropriate biocompatibility and survival, with the highest cell viability seen in the carp nHA scaffolds after 10 days. The results of this study are consistent with the previous studies on the biocompatibility of the scaffolds made up of hydroxyapatite.[60,61] For example, Muhammad et al[60] investigated the biocompatibility of fish scales extracted HA by MTT cell viability assay using Human Embryonic Kidney 293 cells (HEK cells) and epidermoid carcinoma cells (A431 cells). According to their results, the cell viability was greater than 100% for both cell lines. Furthermore, the results of *in vitro* matrix mineralization by Alizarin red staining showed the formation of mineralized nodule in all groups. However, calcium deposition appeared to be higher in human and carp groups**.**

The examination of the biological performance of the scaffolds made from nano hydroxyapatite in the *in vivo* study provides preliminary evidence on the formation of bone tissue. All nHA scaffolds induced complete regeneration of bone lesions in *in vivo* experiments. Interestingly, there was no inflammation around the implanted scaffolds, indicating their high biocompatibility. Usually, a local inflammatory reaction is observed after implantation of orthopedic devices in response to invasive surgery and the presence of a prosthesis.[62] The first contact with the scaffold in the tissue leads to absorption of the protein and formation of a protein layer activates a series of complex controlled responses, including the coagulation cascade, complement system, platelets, and immune cells.[63] This leads to an inflammatory reaction, which should not turn into chronic inflammation, anaphylactic reactions, and consequently loss of body function.[64] The current study demonstrated no evidence of chronic inflammation at histology. In addition, the formation of osteoblast lines, lacunar osteocytes, trabecular and lamellar bone structures, bone marrow, and blood vessels indicated bone regeneration, remodeling, and vascular restoration after 4 and 8 weeks, postoperatively. In all the study groups, bone defects were completely filled with the regenerated bone, with more new bone of higher quality in human extracted nHA after 4 weeks post-surgery. However, the differences between the groups became negligible at week 8. Time exerted a positive effect on bone tissue maturation (elongated osteocytes with lacunae, integration of bone islands, and lamellar bone). Bone regeneration at the critical-size lesion site was complete in all groups, and a very small volume of these materials was observed in the histological examination as demonstrated by the high biodegradation rate of the implanted scaffolds. This contrasts with the characteristics of many materials proposed for bone tissue regeneration, such as polylactic acid and polycaprolactone, which had a much lower rate of degradation.[65,66] Furthermore, the observed *in vivo* degradation rate appeared to be higher rather the in vitro degradation in PBS. After 4 weeks postoperatively, very small magnitude of the scaffolds made from human and carp extracted powders remained at the defect sites, and after 8 weeks the remnants of these scaffolds were very negligible. While, *in vitro*, the means of degradability% were 16.75%, 1.13%, and 0.64%, in respect, for human, carp and commercial groups at day 41. The difference between the *in vivo* and *in vitro* degradation rates can be attributed to the activity of osteoclasts *in vivo*. In one study,[67] the *in vivo* degradation mechanism of hydroxyapatite implanted into sheep bones, was investigated using transmission electron microscopy (TEM). Their finding identified that the osteoclast-mediated degradation of the implanted HA occurred by concurrent resorption and phagocytosis. The authors observed that osteoclasts accumulated closely underneath the HA surface, after 6 weeks of implantation, forming the resorption lacunae and showing ultrastructural characteristics including the ruffled border, the clear zone, and the dorsal microvilli. Furthermore, it has been indicated that the Ca/P ratio and the associated impurities in the calcium phosphate substitutes can influence the *in vitro* biodegradation of HA.[68] Another reason for dissimilar degradation rat between different HA scaffolds may be associated with being synthetic or natural, and the method and source from which the HA was extracted.[69,70]

Previous studies on carp extracted hydroxyapatite concentrated mainly on the method of hydroxyapatite extraction from carp bone as well as the chemical and physical properties of the extracted material, and no

research has been conducted on its use in animals.[18,71,72] In this study, for *in vivo* analysis, the bone repair at the defect site was evaluated through H&E staining. However, it would be interesting to further analyze the new bone formation by immunochemistry and molecular tests, to identify osteogenic and angiogenesis markers and genes. These could be an additional confirmation for histological analysis.

Conclusion

This study, first, the nano hydroxyapatite powders (carp extracted, human extracted, and commercial) were prepared, characterized and used to make bone repairing scaffolds. The scaffolds were subsequently examined for their physicochemical and mechanical properties, cytocompatibility, cell differentiation and *in vivo* ossification. All scaffolds had similar porosity, but different mechanical and degradability behavior. The human nHA scaffolds had the lowest strength and stiffness, and degrade more rapidly. The strength of the scaffolds fabricated by carp extracted and commercial nHA was higher and close to each other, while the stiffness was highest for the scaffolds made from carp extracted nHA. Furthermore, all scaffolds were cytocompatible, where the greatest cell viability rate was in the carp nHA scaffolds after 10 days. Besides, the cell mineralization occurred in all scaffold groups, however, calcium deposition appeared to be higher in human and carp groups. The scaffolds composed of carp and human bone powders had the highest rate of ossification and bone maturation 8 weeks after surgery. The tissue response rate to these scaffolds was higher than that of commercial nHA powder at both 4 and 8 weeks postoperatively. Therefore, these scaffolds can be promising for clinical applications. In addition, the carp-extracted nano-hydroxyapatite powder can be used for scaffolding and coating of orthopedic and dental implants.

Acknowledgements

The authors would like to thank Semnan University of Medical Sciences for funding this work (NO. 1713).

Authors' Contribution

Conceptualization: Marjan Bahraminasab, Akram Alizadeh.
Data curation: Marjan Bahraminasab.
Formal analysis: Marjan Bahraminasab, Mohammad Yousefi.
Funding acquisition: Marjan Bahraminasab.
Investigation: Mohammad Yousefi, Samaneh Arab.
Methodology: Mohammad Yousefi, Athar Talebi, Ali Ghanbari, Marjan Bahraminasab, Muhammad Mehdi Jafari Sorkhdehi.
Project administration: Marjan Bahraminasab, Samaneh Arab.
Resources: Marjan Bahraminasab.
Supervision: Marjan Bahraminasab.
Validation: Marjan Bahraminasab, Samaneh Arab.
Visualization: Mohammad Yousefi, Marjan Bahraminasab.
Writing-original draft: Mohammad Yousefi, Marjan Bahraminasab.
Writing-review & editing: Marjan Bahraminasab, Nicola Maffulli, Samaneh Arab.

Competing Interests

The authors declare that they have no conflict of interest.

Research Highlights

- The extraction of nano-hydroxyapatite from carp bone waste is cost-effective, and can reduce the cost of bone repair or replacement.
- The carp extracted nHA scaffolds showed comparable osteogenic properties to those of human-derived and have the potential for clinical applications.

Ethical Approval

The animal experimental protocol was approved by the Ethical Review Board of Semnan University of Medical Sciences (Ethic code: IR.SEMUMS.REC.1398.273).

Funding

This study was funded by Semnan University of Medical Sciences (NO. 1713).

References

1. Bahraminasab M, Janmohammadi M, Arab S, Talebi A, Taghdiri Nooshabadi V, Koohsarian P, et al. Bone scaffolds: an incorporation of biomaterials, cells, and biofactors. *ACS Biomater Sci Eng* **2021**; 7: 5397-431. doi: 10.1021/acsbiomaterials.1c00920.
2. Burg KJ, Porter S, Kellam JF. Biomaterial developments for bone tissue engineering. *Biomaterials* **2000**; 21: 2347-59. doi: 10.1016/s0142-9612(00)00102-2.
3. Wang W, Yeung KW. Bone grafts and biomaterials substitutes for bone defect repair: a review. *Bioact Mater* **2017**; 2: 224-47. doi: 10.1016/j.bioactmat.2017.05.007.
4. Selim M, Mousa HM, Abdel-Jaber GT, Barhoum A, Abdal-hay A. Innovative designs of 3D scaffolds for bone tissue regeneration: Understanding principles and addressing challenges. *European Polymer Journal.* **2024**:215;113251. doi: 10.1016/j.eurpolymj.2024.113251.
5. Roseti L, Parisi V, Petretta M, Cavallo C, Desando G, Bartolotti I, et al. Scaffolds for bone tissue engineering: state of the art and new perspectives. *Mater Sci Eng C Mater Biol Appl* **2017**; 78: 1246-62. doi: 10.1016/j.msec.2017.05.017.
6. Bahraminasab M, Edwards KL. Biocomposites for hard tissue replacement and repair. In: Sidhu SS, Bains PS, Zitoune R, Yazdani M, eds. *Futuristic Composites: Behavior, Characterization, and Manufacturing*. Singapore: Springer; **2018**. p. 281-96. doi: 10.1007/978-981-13-2417-8_14.
7. Bahraminasab M, Edwards KL. Computational tailoring of orthopaedic biomaterials: design principles and aiding tools. In: Bains PS, Sidhu SS, Bahraminasab M, Prakash C, eds. *Biomaterials in Orthopaedics and Bone Regeneration: Design and Synthesis*. Singapore: Springer; **2019**. p. 15-31. doi: 10.1007/978-981-13-9977-0_2.
8. Loh QL, Choong C. Three-dimensional scaffolds for tissue engineering applications: role of porosity and pore size. *Tissue Eng Part B Rev* **2013**; 19: 485-502. doi: 10.1089/ten.TEB.2012.0437.
9. Liu P, Li Z, Zhu M, Sun Y, Li Y, Wang H, et al. Preparation of EGFR monoclonal antibody conjugated nanoparticles and targeting to hepatocellular carcinoma. *J Mater Sci Mater Med* **2010**; 21: 551-6. doi: 10.1007/s10856-009-3925-8.
10. Kang X, Zhang W, Yang C. Mechanical properties study of micro- and nano-hydroxyapatite reinforced ultrahigh molecular weight polyethylene composites. *J Appl Polym Sci* **2016**; 133. doi: 10.1002/app.42869.
11. Harris PA, Taylor R, Minor BL, Elliott V, Fernandez M, O'Neal L, et al. The REDCap consortium: building an international community of software platform partners. *J Biomed Inform* **2019**; 95: 103208. doi: 10.1016/j.jbi.2019.103208.
12. Spicer PP, Kretlow JD, Young S, Jansen JA, Kasper FK, Mikos AG. Evaluation of bone regeneration using the rat critical size calvarial defect. *Nat Protoc* **2012**; 7: 1918-29. doi: 10.1038/nprot.2012.113.
13. Hoyer B, Bernhardt A, Heinemann S, Stachel I, Meyer M, Gelinsky

M. Biomimetically mineralized salmon collagen scaffolds for application in bone tissue engineering. *Biomacromolecules* **2012**; 13: 1059-66. doi: 10.1021/bm201776r.
14. Boutinguiza M, Pou J, Comesaña R, Lusquiños F, de Carlos A, León B. Biological hydroxyapatite obtained from fish bones. *Mater Sci Eng C Mater Biol Appl* **2012**; 32: 478-86. doi: 10.1016/j.msec.2011.11.021.
15. da Cruz JA, Weinand WR, Neto AM, Palácios RS, Sales AJ, Prezas PR, et al. Low-cost hydroxyapatite powders from tilapia fish. *JOM* **2020**; 72: 1435-42. doi: 10.1007/s11837-019-03998-4.
16. Hammood AS, Hassan SS, Alkhafagy MT, Jaber HL. Effect of calcination temperature on characterization of natural hydroxyapatite prepared from carp fish bones. *SN Appl Sci* **2019**; 1: 436. doi: 10.1007/s42452-019-0396-5.
17. Granito RN, Muniz Renno AC, Yamamura H, de Almeida MC, Menin Ruiz PL, Ribeiro DA. Hydroxyapatite from fish for bone tissue engineering: a promising approach. *Int J Mol Cell Med* **2018**; 7: 80-90. doi: 10.22088/ijmcm.Bums.7.2.80.
18. Bahraminasab M, Doostmohammadi N, Alizadeh A. Low-cost synthesis of nano-hydroxyapatite from carp bone waste: effect of calcination time and temperature. *Int J Appl Ceram Technol* **2021**; 18: 573-82. doi: 10.1111/ijac.13678.
19. Minim PR, de Azevedo-Silva LJ, Ferrairo BM, Pereira LF, Goulart CA, Monteiro-Sousa RS, et al. The combined effects of binder addition and different sintering methods on the mechanical properties of bovine hydroxyapatite. *J Mech Behav Biomed Mater* **2023**; 144: 105993. doi: 10.1016/j.jmbbm.2023.105993.
20. Indra A, Setiawan R, Mulyadi I, Affi J, Gunawarman G. The effect of PVA addition as binders on the properties of hydroxyapatite sintered body. In: Proceedings of the 2nd International Conference on Industrial and Technology and Information Design, ICITID 2021, 30 August 2021, Yogyakarta, Indonesia. EAI; **2021**. doi: 10.4108/eai.30-8-2021.2311514.
21. Wang J, Wu D, Zhang Z, Li J, Shen Y, Wang Z, et al. Biomimetically ornamented rapid prototyping fabrication of an apatite-collagen-polycaprolactone composite construct with nano-micro-macro hierarchical structure for large bone defect treatment. *ACS Appl Mater Interfaces* **2015**; 7: 26244-56. doi: 10.1021/acsami.5b08534.
22. Bahraminasab M, Sahari BB, Edwards KL, Farahmand F, Hong TS, Naghibi H. Material tailoring of the femoral component in a total knee replacement to reduce the problem of aseptic loosening. *Mater Des* **2013**; 52: 441-51. doi: 10.1016/j.matdes.2013.05.066.
23. Xia Z, Yu X, Jiang X, Brody HD, Rowe DW, Wei M. Fabrication and characterization of biomimetic collagen-apatite scaffolds with tunable structures for bone tissue engineering. *Acta Biomater* **2013**; 9: 7308-19. doi: 10.1016/j.actbio.2013.03.038.
24. Bahraminasab M, Arab S, Jahan A. Adaptation of MC3T3 cell line to Dulbecco's Modified Eagle's medium. *Tissue Cell* **2020**; 64: 101341. doi: 10.1016/j.tice.2020.101341.
25. Bahraminasab M, Arab S, Safari M, Talebi A, Kavakebian F, Doostmohammadi N. In vivo performance of Al2O3-Ti bone implants in the rat femur. *J Orthop Surg Res* **2021**; 16: 79. doi: 10.1186/s13018-021-02226-7.
26. Abidi SS, Murtaza Q. Synthesis and characterization of nano-hydroxyapatite powder using wet chemical precipitation reaction. *J Mater Sci Technol* **2014**; 30: 307-10. doi: 10.1016/j.jmst.2013.10.011.
27. Chandrasekar A, Sagadevan S, Dakshnamoorthy A. Synthesis and characterization of nano-hydroxyapatite (n-HAP) using the wet chemical technique. *Int J Phys Sci* **2013**; 8: 1639-45. doi: 10.5897/ijps2013.3990.
28. Cardoso GB, Chacon EL, Maia LR, de Carvalho Zavaglia CA, da Cunha MR. The importance of understanding differences in a critical size model: a preliminary in vivo study using tibia and parietal bone to evaluate the reaction with different biomaterials. *Mater Res* **2018**; 22: e20180491. doi: 10.1590/1980-5373-mr-2018-0491.
29. Dorozhkina EI, Dorozhkin SV. Mechanism of the solid-state transformation of a calcium-deficient hydroxyapatite (CDHA) into biphasic calcium phosphate (BCP) at elevated temperatures. *Chem Mater* **2002**; 14: 4267-72. doi: 10.1021/cm0203060.
30. Douglas TE, Schietse J, Zima A, Gorodzha S, Parakhonskiy BV, KhaleNkow D, et al. Novel self-gelling injectable hydrogel/alpha-tricalcium phosphate composites for bone regeneration: Physiochemical and microcomputer tomographical characterization. *J Biomed Mater Res A* **2018**; 106: 822-8. doi: 10.1002/jbm.a.36277.
31. Jang HL, Zheng GB, Park J, Kim HD, Baek HR, Lee HK, et al. In vitro and in vivo evaluation of whitlockite biocompatibility: comparative study with hydroxyapatite and β-tricalcium phosphate. *Adv Healthc Mater* **2016**; 5: 128-36. doi: 10.1002/adhm.201400824.
32. Moreno D, Vargas F, Ruiz J, López ME. Solid-state synthesis of alpha tricalcium phosphate for cements used in biomedical applications. *Bol Soc Esp Cerám Vidr* **2020**; 59: 193-200. doi: 10.1016/j.bsecv.2019.11.004.
33. Reyes-Gasga J, Becerril NV. Electron microscopy analysis of the thermal phase transition from hydroxyapatita to β-TCP observed in human teeth. *J Microsc* **2019**; 276: 89-97. doi: 10.1111/jmi.12839.
34. Stoia M, Ionescu M, Stef O, Murgan R, Stefanescu M. Preparation of β-tricalcium phosphate from precursors obtained by a wet precipitation method. *Chem Bull POLITEHNICA Univ Timisoara* **2008**; 53: 1-2.
35. Clarke B. Normal bone anatomy and physiology. *Clin J Am Soc Nephrol* **2008**; 3 Suppl 3: S131-9. doi: 10.2215/cjn.04151206.
36. Calasans-Maia MD, de Melo BR, Alves AT, de Brito Resende RF, Louro RS, Sartoretto SC, et al. Cytocompatibility and biocompatibility of nanostructured carbonated hydroxyapatite spheres for bone repair. *J Appl Oral Sci* **2015**; 23: 599-608. doi: 10.1590/1678-775720150122.
37. Reyes-Gasga J, Martínez-Piñeiro EL, Rodríguez-Álvarez G, Tiznado-Orozco GE, García-García R, Brès EF. XRD and FTIR crystallinity indices in sound human tooth enamel and synthetic hydroxyapatite. *Mater Sci Eng C Mater Biol Appl* **2013**; 33: 4568-74. doi: 10.1016/j.msec.2013.07.014.
38. Londoño-Restrepo SM, Jeronimo-Cruz R, Rubio-Rosas E, Rodriguez-García ME. The effect of cyclic heat treatment on the physicochemical properties of bio hydroxyapatite from bovine bone. *J Mater Sci Mater Med* **2018**; 29: 52. doi: 10.1007/s10856-018-6061-5.
39. Zhang L, Zhang C, Zhang R, Jiang D, Zhu Q, Wang S. Extraction and characterization of HA/β-TCP biphasic calcium phosphate from marine fish. *Mater Lett* **2019**; 236: 680-2. doi: 10.1016/j.matlet.2018.11.014.
40. Zhu Q, Ablikim Z, Chen T, Cai Q, Xia J, Jiang D, et al. The preparation and characterization of HA/β-TCP biphasic ceramics from fish bones. *Ceram Int* **2017**; 43: 12213-20. doi: 10.1016/j.ceramint.2017.06.082.
41. Chesley M, Kennard R, Roozbahani S, Kim SM, Kukk K, Mason M. One-step hydrothermal synthesis with in situ milling of biologically relevant hydroxyapatite. *Mater Sci Eng C Mater Biol Appl* **2020**; 113: 110962. doi: 10.1016/j.msec.2020.110962.
42. Lü XY, Fan YB, Gu D, Cui W. Preparation and characterization of natural hydroxyapatite from animal hard tissues. *Key Eng Mater* **2007**;342-343:213-6. doi: 10.4028/www.scientific.net/KEM.342-343.213.
43. Geng Z, Yuan Q, Zhuo X, Li Z, Cui Z, Zhu S, et al. Synthesis, characterization, and biological evaluation of nanostructured hydroxyapatite with different dimensions. *Nanomaterials (Basel)* **2017**; 7: 38. doi: 10.3390/nano7020038.
44. Chen CH, Pei X, Tulu US, Aghvami M, Chen CT, Gaudillière D, et al. A comparative assessment of implant site viability in humans and rats. *J Dent Res* **2018**; 97: 451-9. doi: 10.1177/0022034517742631.
45. Figueiredo MM, Gamelas JA, Martins AG. Characterization of bone and bone-based graft materials using FTIR spectroscopy. In: Theophanides T, ed. *Infrared Spectroscopy-Life and Biomedical Sciences*. IntechOpen; **2012**. p. 315-38. doi: 10.5772/36379.
46. Yadav U, Saxena PS, Srivastava A. Simple route synthesis of

hydroxyapatite–gelatin nanocomposite and its characterization. *Int J Mater Sci* **2017**; 12: 1-3. doi: 10.13140/rg.2.2.17856.43525.
47. Mishra VK, Srivastava SK, Asthana BP, Kumar D. Structural and spectroscopic studies of hydroxyapatite nanorods formed via microwave-assisted synthesis route. *J Am Ceram Soc* **2012**; 95: 2709-15. doi: 10.1111/j.1551-2916.2012.05134.x.
48. Kandić L, Mitrić M, Ignjatović N. XRD analysis of calcium phosphate and biocomposite calcium phosphate/bioresorbable polymer. *Mater Sci Forum* **2006**; 518: 507-12. doi: 10.4028/www.scientific.net/MSF.518.507.
49. Dudek K, Szaraniec B, Lelątko J, Goryczka T. Structure of multi-layers deposited on NiTi shape memory alloy. *Solid State Phenom* **2013**; 203-204: 90-3. doi: 10.4028/www.scientific.net/SSP.203-204.90.
50. Saeed GK, Essa AF, Said SA. Preparation and characterization of hydroxyapatite powder and study of hydroxyapatite-alumina composite. *J Phys Conf Ser* **2020**; 1591: 012006. doi: 10.1088/1742-6596/1591/1/012006.
51. Venkatesan J, Kim SK. Effect of temperature on isolation and characterization of hydroxyapatite from tuna (*Thunnus obesus*) bone. *Materials (Basel)* **2010**; 3: 4761-72. doi: 10.3390/ma3104761.
52. Youseflee P, Esmaeili Ranjbar F, Bahraminasab M, Ghanbari A, Rabiei Faradonbeh D, Arab S, et al. Exosome loaded hydroxyapatite (HA) scaffold promotes bone regeneration in calvarial defect: an in vivo study. *Cell Tissue Bank* **2023**; 24: 389-400. doi: 10.1007/s10561-022-10042-4.
53. Hannora AE, Mukasyan AS, Mansurov ZA. Mechanochemical synthesis of nanocrystalline hydroxyapatite coating. *Eurasian Chem Technol J* **2010**; 12: 79-95. doi: 10.18321/ectj30.
54. Duraia ES, Hannora A, Mansurov Z, Beall GW. Direct growth of carbon nanotubes on hydroxyapatite using MPECVD. *Mater Chem Phys* **2012**; 132: 119-24. doi: 10.1016/j.matchemphys.2011.11.006.
55. Madhukumar K, Varma HK, Komath M, Elias TS, Padmanabhan V, Nair CM. Photoluminescence and thermoluminescence properties of tricalcium phosphate phosphors doped with dysprosium and europium. *Bull Mater Sci* **2007**; 30: 527-34. doi: 10.1007/s12034-007-0082-x.
56. Abbasi N, Hamlet S, Love RM, Nguyen N-T. Porous scaffolds for bone regeneration. *J Sci Adv Mater Devices* **2020**; 5: 1-9. doi: 10.1016/j.jsamd.2020.01.007.
57. Shim JH, Jeong JH, Won JY, Bae JH, Ahn G, Jeon H, et al. Porosity effect of 3D-printed polycaprolactone membranes on calvarial defect model for guided bone regeneration. *Biomed Mater* **2017**; 13: 015014. doi: 10.1088/1748-605X/aa9bbc.
58. Sotiropoulou P, Fountos G, Martini N, Koukou V, Michail C, Kandarakis I, et al. Bone calcium/phosphorus ratio determination using dual energy X-ray method. *Phys Med* **2015**; 31: 307-13. doi: 10.1016/j.ejmp.2015.01.019.
59. Hannink G, Arts JJ. Bioresorbability, porosity and mechanical strength of bone substitutes: what is optimal for bone regeneration? *Injury* **2011**; 42 Suppl 2: S22-5. doi: 10.1016/j.injury.2011.06.008.
60. Muhammad N, Gao Y, Iqbal F, Ahmad P, Ge R, Nishan U, et al. Extraction of biocompatible hydroxyapatite from fish scales using novel approach of ionic liquid pretreatment. *Sep Purif Technol* **2016**; 161: 129-35. doi: 10.1016/j.seppur.2016.01.047.
61. Fu Q, Rahaman MN, Bal BS, Brown RF. In vitro cellular response to hydroxyapatite scaffolds with oriented pore architectures. *Mater Sci Eng C Mater Biol Appl* **2009**; 29: 2147-53. doi: 10.1016/j.msec.2009.04.016.
62. Brooks EK, Brooks RP, Ehrensberger MT. Effects of simulated inflammation on the corrosion of 316L stainless steel. *Mater Sci Eng C Mater Biol Appl* **2017**; 71: 200-5. doi: 10.1016/j.msec.2016.10.012.
63. Gorbet MB, Sefton MV. Biomaterial-associated thrombosis: roles of coagulation factors, complement, platelets and leukocytes. *Biomaterials* **2004**; 25: 5681-703. doi: 10.1016/j.biomaterials.2004.01.023.
64. Franz S, Rammelt S, Scharnweber D, Simon JC. Immune responses to implants - a review of the implications for the design of immunomodulatory biomaterials. *Biomaterials* **2011**; 32: 6692-709. doi: 10.1016/j.biomaterials.2011.05.078.
65. Asti A, Gioglio L. Natural and synthetic biodegradable polymers: different scaffolds for cell expansion and tissue formation. *Int J Artif Organs* **2014**; 37: 187-205. doi: 10.530/ijao.5000307.
66. Mao D, Li Q, Li D, Chen Y, Chen X, Xu X. Fabrication of 3D porous poly(lactic acid)-based composite scaffolds with tunable biodegradation for bone tissue engineering. *Mater Des* **2018**; 142: 1-10. doi: 10.1016/j.matdes.2018.01.016.
67. Wenisch S, Stahl JP, Horas U, Heiss C, Kilian O, Trinkaus K, et al. In vivo mechanisms of hydroxyapatite ceramic degradation by osteoclasts: fine structural microscopy. *J Biomed Mater Res A* **2003**; 67: 713-8. doi: 10.1002/jbm.a.10091.
68. Wang H, Lee JK, Moursi A, Lannutti JJ. Ca/P ratio effects on the degradation of hydroxyapatite in vitro. *J Biomed Mater Res A* **2003**; 67: 599-608. doi: 10.1002/jbm.a.10538.
69. Mezahi F, Oudadesse H, Harabi A, Lucas-Girot A, Le Gal Y, Chaair H, et al. Dissolution kinetic and structural behaviour of natural hydroxyapatite vs. thermal treatment: comparison to synthetic hydroxyapatite. *J Therm Anal Calorim* **2009**; 95: 21-9. doi: 10.1007/s10973-008-9065-4.
70. Firdaus Hussin MS, Abdullah HZ, Idris MI, Abdul Wahap MA. Extraction of natural hydroxyapatite for biomedical applications-a review. *Heliyon* **2022**; 8: e10356. doi: 10.1016/j.heliyon.2022.e10356.
71. Liu Y, Li J, Wang D, Yang F, Zhang L, Ji S, et al. Enhanced extraction of hydroxyapatite from bighead carp (*Aristichthys nobilis*) scales using deep eutectic solvent. *J Food Sci* **2020**; 85: 150-6. doi: 10.1111/1750-3841.14971.
72. Liu Y, Liu M, Ji S, Zhang L, Cao W, Wang H, et al. Preparation and application of hydroxyapatite extracted from fish scale waste using deep eutectic solvents. *Ceram Int* **2021**; 47: 9366-72. doi: 10.1016/j.ceramint.2020.12.067.